JACS
JOURNAL OF THE AMERICAN CHEMICAL SOCIETY

Article

pubs.acs.org/JACS

Organization and Dynamics of Receptor Proteins in a Plasma Membrane

Heidi Koldsø*,† and Mark S. P. Sansom*

Department of Biochemistry, University of Oxford, South Parks Road, Oxford OX1 3QU, United Kingdom

Supporting Information

ABSTRACT: The interactions of membrane proteins are influenced by their lipid environment, with key lipid species able to regulate membrane protein function. Advances in high-resolution microscopy can reveal the organization and dynamics of proteins and lipids within living cells at resolutions <200 nm. Parallel advances in molecular simulations provide near-atomic-resolution models of the dynamics of the organization of membranes of *in vivo*-like complexity. We explore the dynamics of proteins and lipids in crowded and complex plasma membrane models, thereby closing the gap in length and complexity between computations and experiments. Our simulations provide insights into the mutual interplay between lipids and proteins in determining mesoscale (20−100 nm) fluctuations of the bilayer, and in enabling oligomerization and clustering of membrane proteins.

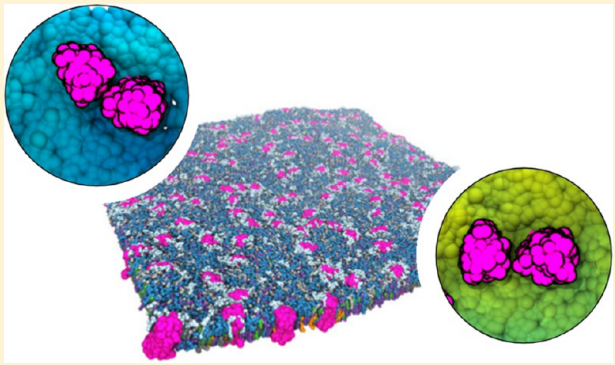

INTRODUCTION

Cell membranes are crowded and spatially heterogeneous environments for proteins. Recent advances in lipidomics have provided insights into the diversity of lipids and their biological roles.[1,2] The composition of a cell membrane depends on the cell type and also on the organelle in which it is present.[3] Thus, the human plasma membrane (PM) is composed of glycerolipids, sphingolipids, and sterols, including cholesterol (Chol), and the composition of the lipids within the PM is asymmetric between the outer and inner leaflets.[2−8] The outer leaflet is composed mostly of phosphatidylcholine (PC) and sphingomyelin (Sph), along with glycosphingolipids such as monosialodihexosylganglioside (GM3), and also Chol. The inner leaflet also contains Chol, alongside phosphoethanolamine (PE), phosphoserine (PS), and phosphatidylinositols (PIs) such as phosphatidylinositol-4,5-bisphosphate (PIP_2). The presence of PS and PIs results in the inner leaflet of the PM being anionic in nature.[3−5,9] In conjunction with improved descriptions of their compositional complexity, it becomes increasingly evident that cell membranes do not function simply as a barrier between cellular compartments, but are involved in regulation of membrane protein function, in membrane trafficking, and in membrane compartmentalization via formation of lipid nano-domains/rafts.[3,10−15]

Recent advances in super-resolution microscopy have resulted in a greatly improved understanding of the dynamic localization of proteins and lipids within the membranes of living cells.[7,16−19] For example, high-resolution methodologies such as stimulated emission depletion (STED) microscopy have revealed the heterogeneity of organization of both lipids and proteins within cell membranes at resolutions <200 nm.[16,17,19−21] In parallel with developments in cell imaging, computational approaches now enable us to explore in detail the structural and dynamic properties of model membranes.[22] However, computer simulation studies of membranes have only recently moved toward development of more biologically realistic membrane models.[23−26] This has allowed us and others to explore, for example, the formation of lipid nanodomains within PM models,[23,25] and the ability of receptors to induce local lipid clusters.[24,27]

Coarse-grained (CG) molecular dynamics (MD) simulations, as exemplified by the MARTINI methodology,[28−30] are capable of modeling *in vivo* membrane complexity,[23,25,26] and also, in principle, of approaching experimental length scales of 100 nm and above. Here we present the first such studies that close the gap in length and complexity between simulations and experiments such as super-resolution microscopy. We have constructed CG models that model key aspects of compositional complexity and molecular crowding within a mammalian PM, at length scales >100 nm and thus directly comparable with current experimental approaches. We explore the behavior of complex asymmetric PM models with and without two types of crowded membrane proteins present. These simulations reveal lipid-mediated oligomerization of proteins into nanoscale domains, accompanied by reduction of the diffusion rates of proteins and lipids. This indicates that complexities in lateral organization are intrinsic and emergent properties of complex and crowded cell membranes, independent of but open to

Received: August 6, 2015
Published: October 30, 2015

DOI: 10.1021/jacs.5b08048
J. Am. Chem. Soc. 2015, 137, 14694−14704

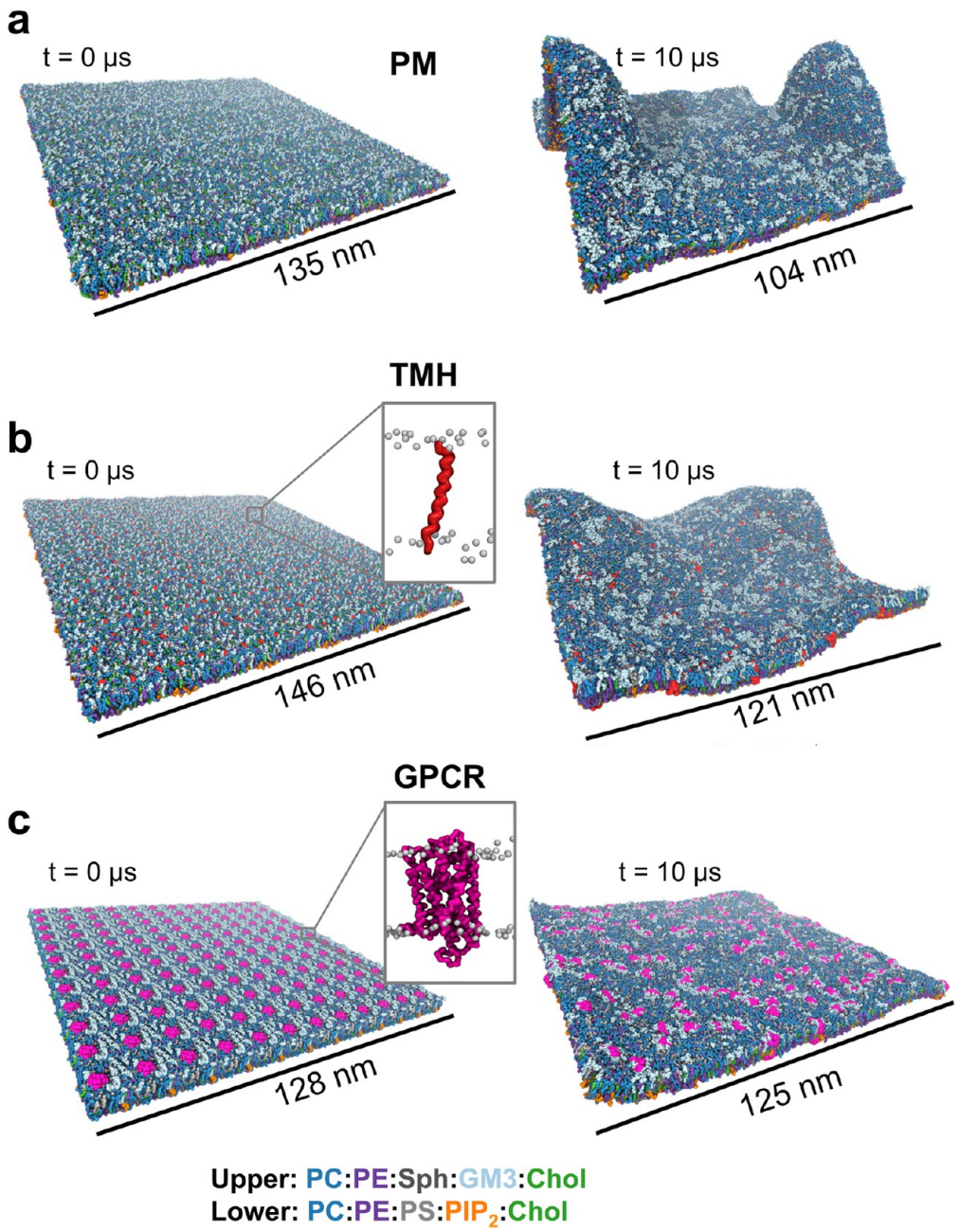

Figure 1. Membrane models at the start and end of the 10 μs simulations. PC is shown in dark blue, PE in purple, Sph in dark gray, GM3 in light blue, Chol in green, PS in light gray, and PIP_2 in orange. (a) **PM** model without any proteins, consisting of 54 000 lipids. (b) **TMH** system, containing 576 repeats of a single TM helix (in red) from the gp130 cytokine receptor and 63 342 lipids. (c) **GPCR** system, containing 144 repeats of the S1P1 receptor (in pink) and 59 616 lipids.

modulation by interactions of membrane proteins with the underlying cytoplasmic cytoskeleton.

METHODS

Setup of the PM System. The model consisted of a plasma membrane-like lipid mixture, with an outer leaflet composed of PC:PE:Sph:GM3:Chol (40:10:15:10:25) and an inner leaflet of PC:PE:PS:PIP_2:Chol (10:40:15:10:25). PC, PE, and PS were modeled with 1-palmitoyl-2-oleoyl (PO) lipid tails (i.e., each with one unsaturated bead), while Sph and GM3 were modeled with the ceramide tail with one unsaturated bead. PIP_2 was modeled using a fully saturated tail. The **PM** model without any proteins consisted of 54 000 lipids, as was built from a 6000-lipid PM model described earlier.[23] The 6000-lipid patch was constructed from a pure PC bilayer that was converted into the desired asymmetric membrane model either by renaming and thereby exchanging lipids the same size as or smaller than PC or by alignment and substitution for larger lipids (such as GM3 and PIP_2), as described previously by Koldsø et al.[23] The 6000-lipid patch was concatenated onto a 3×3 system, resulting in a 54 000-lipid system with a PM-like composition. The standard MARTINI water model was used, and the system was neutralized using NaCl to a 0.15 M concentration. The resultant system consisted of a total of 2.28×10^6 particles (see also Table S1). The parameters for PC, PE, PS, Sph, and Chol were obtained from the MARTINI webpage (http://md.chem.rug.nl/cgmartini/images/parameters/ITP/martini_v2.0_lipids.itp), while parametrization of GM3 and PIP_2 has been described previously[23,31]

Setup of the TMH System. The transmembrane (TM) domain of gp130 was modeled in PyMOL (PyMOL Molecular Graphics System,

DOI: 10.1021/jacs.5b08048
J. Am. Chem. Soc. 2015, 137, 14694−14704

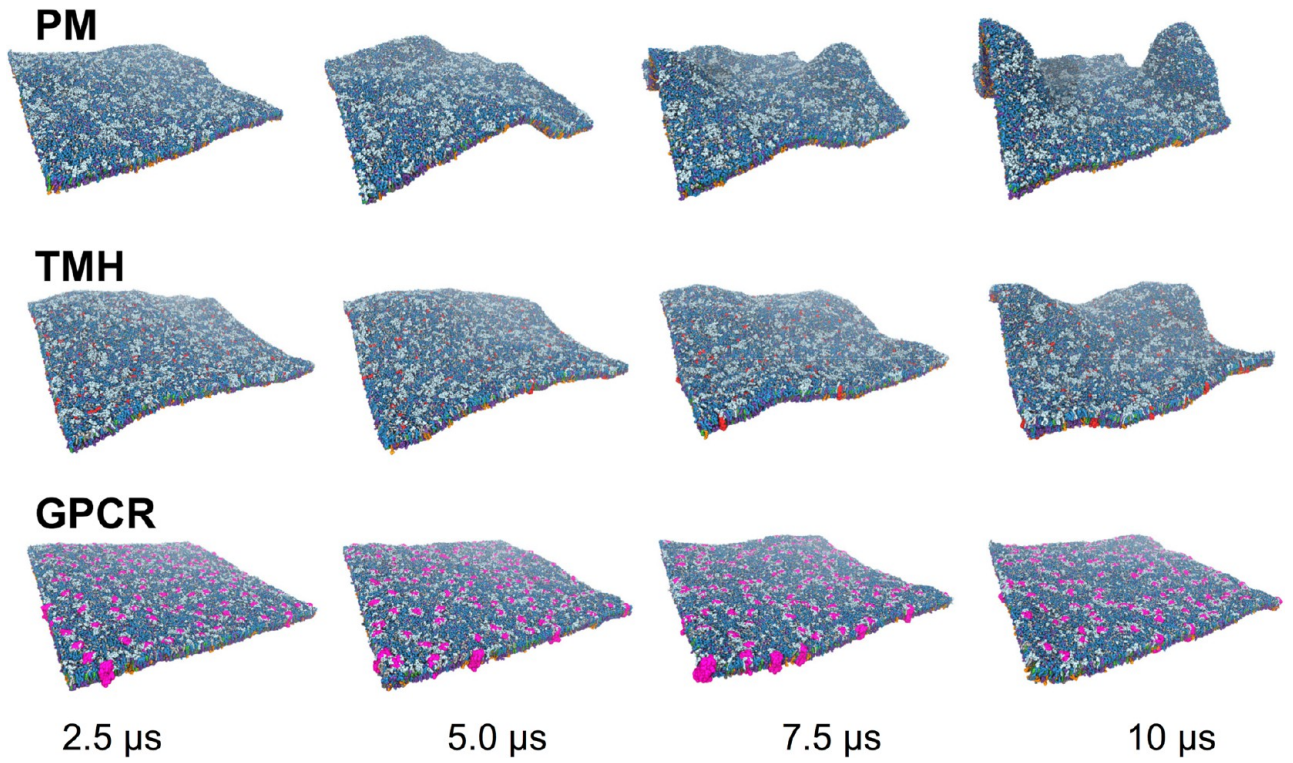

Figure 2. Dynamic evolution of membrane models. Evolution of membrane fluctuations over time is illustrated with snapshots at 2.5, 5.0, 7.5, and 10 μs simulation times for the **PM**, **TMH**, and **GPCR** systems. Colors are as in Figure 1; the complete 10 μs simulations are shown in Movies S1–S3.

Version 1.5.0.4 Schrödinger, LLC) as previously described[23,27] and converted into CG representation using the MARTINI2.2[28] force field. The **TMH** system was constructed based on concatenating a 6×6 system containing 16 gp130 TM helixes within a PM model (see above) consisting of 1756 lipids as described previously.[23] The resulting system consisted of 576 copies of the gp130 TM helix and 63 342 lipids. The standard MARTINI water model was applied, and the system was neutralized using a NaCl concentration of 0.15 M, which yielded a total of 2.69×10^6 particles (see also Table S1).

Setup of the GPCR System. The structure of the sphingosine 1-phosphate receptor 1 (S1P1) G-protein-coupled receptor (GPCR) was derived from PDB code 3V2W.[32] The T4 lysozyme insert used in the structure determination was removed, and missing residues 12–16, 40–46, 149–155, 232–243, and 326–330 were modeled using Modeller 9.10,[33] which yielded a protein model consisting of residues 12–330. Additionally, the genome sequence (K250, S251, L252) from UNIPROT (P21453) was used instead of the NV sequence from the epithelium used by the authors of the crystal structure.[32] The atomistic S1P1 receptor model was energy minimized using a steepest descent method prior to being converted into CG representation using the MARTINI2.2 force field and the ELNEDYN[34] elastic network model. A single CG model of S1P1 was embedded into a PC bilayer through a 25 ns self-assembly simulation.[35] The PC membrane was subsequently converted into a PM model utilizing the in-house exchange lipid methodology (see above) to the same composition as the **PM** model. The system containing the S1P1 receptor embedded into a PM model was then equilibrated for 10 ns prior to being concatenated into a 12 × 12 system. The resulting system contained 144 repeats of the S1P1 receptor proteins, 59 616 lipids, and was solvated with the standard MARTINI water model and neutralized to a 0.15 M NaCl concentration. The **GPCR** system thus contained 2.60×10^6 particles (see also Table S1).

Coarse-Grained Molecular Dynamics Simulations. All simulations were performed using GROMACS 4.6[36] (www.gromacs.org) and the standard MARTINI protocol. Periodic boundary conditions were applied, and a time step of 20 fs was applied in all the simulations. The temperature was maintained at 323 K using a Berendsen thermostat,[37] and the pressure at 1 bar using a Berendensen barostat. For both the temperature and pressure, a coupling constant of 1 ps was used for the **PM** and **TMH** systems, while a coupling constant of 4 ps was used for the **GPCR** system. In all simulations the reaction field coulomb type was used with a switching function from 0.0 to 1.2 nm, and the van der Waals interactions were treated using a cutoff with a switching function from 0.9 to 1.2 nm. The LINCS algorithm was used to constrain covalent bonds to their equilibrium values.[38] All three systems were simulated for 10 μs of production run.

Analysis. Diffusion coefficients were calculated from the mean-square displacement at various intervals through *g_msd*, using a time step of 5 ns, and the density distributions of lipid headgroups were obtained through *g_density*, both in GROMACS. VMD plugins were used to compute radial distribution functions.[39,40] Contact data were obtained from in-house scripts and visualization in VMD.[40] The protein cluster analysis was based on MDAnalysis[41] and in-house scripts.

RESULTS

Three Dynamic Membrane Systems. Three large (ca. 140 × 140 nm^2; see Table S1 for details) plasma membrane model systems were constructed (Figure 1). Each of these was based upon an asymmetric lipid bilayer. The composition of the extracellular leaflet was PC:PE:Sph:GM3:Chol = 40:10:15:10:25, and that of the intracellular leaflet was PC:PE:PS:PIP_2:Chol = 10:40:15:10:25.

The first system was a plasma membrane (**PM**, Figure 1a) lipid bilayer without any proteins present. This provided a control for comparison with two systems containing multiple copies of proteins at biologically relevant degrees of crowding. A simple protein-containing system (**TMH**, Figure 1b), based on previous smaller-scale studies,[23] contained 576 copies of a single α-helical TM domain (that of the gp130 cytokine receptor) including short (4 residue) juxtamembrane (JM) domains on each side of the membrane. In this system the

DOI: 10.1021/jacs.5b08048
J. Am. Chem. Soc. 2015, 137, 14694–14704

protein occupied approximately 6% of the cross-sectional area of the membrane. A more complex model (**GPCR**, Figure 1c) was constructed from a large PM patch into which 144 copies of a GPCR, the proteins thus occupying 12% of the area of the membrane. This enabled us to probe the nanoscale organization and dynamics of a pharmaceutically important GPCR, S1P1 (PDB code 3V2W).[32] The S1P1 receptor is a target for the lipid-like drug fingolimod, which is used to treat multiple sclerosis.[42]

Each of the three membrane systems was simulated for 10 μs. Substantial differences in the dynamic behavior of the membranes were observed based on the presence or absence of membrane proteins and on the nature and degree of crowding of the protein incorporated (Figures 1 and 2; Movies S1–S3). In particular, it is evident that the degree of local curvature and membrane dynamics are strongly dependent on the nature of the simulation system. Within the **PM** model without proteins, we observed large-scale membrane curvature/deformation (Figures 1a and S1). This degree of local membrane deformation is suggestive of incipient budding and/or tubulation of the (asymmetric) membrane, but as neither proteins nor an underlying cytoskeleton is present, it may be more representative of *in vitro* than of *in vivo* behavior of cell membranes. Examination of the **TMH** and **GPCR** simulations indicates that the presence of (crowded) membrane proteins stabilized the fluctuation and curvature of the membrane, with a greater degree of stabilization of planarity correlating with an increased degree of crowding, such that the bilayer fluctuates less in the **GPCR** system (ca. 12% protein) than in the **TMH** system (ca. 6% protein).

Membrane Area Per Lipid. All simulations started from a planar membrane model. To ensure that the area per lipid is the same in both leaflets of the asymmetric bilayers we tested the area per lipid for the different lipid species as described previously.[23] We have now extended this analysis, using APL@Voroni[43] to evaluate area per lipid for each of the different lipid species in the different bilayers. This analysis (summarized in Table S2 and Figures S2–S7) shows that the area per lipid overall and the area for each lipid species are the same for both symmetric and asymmetric membrane simulations. (Each condition was tested using simulations of small bilayers of 1500 lipids with the same lipid composition as the large PM system.) Hence we are confident that the dynamics and curvature of the membranes during simulations do not arise from differences in area per lipid between the two leaflets of the PM and derived models.

Additionally we calculated the average area per lipid of each lipid species within the **PM**, **TMH**, and **GPCR** systems over the initial period (1–3 μs) of the three simulations (Table S3). Overall we see the same average areas per lipid for each lipid species when compared to a smaller protein-free PM model (Table S2, Figures S6 and S7). The largest difference observed is for PIP_2, which has a lower area within the **GPCR** system, most likely a result of tight local clustering of this lipid around the protein when the GPCR is present (see below).

Membrane Fluctuations and Deformations. Significant fluctuations were observed within the first few microseconds and continued throughout the simulation (Figure 2). Comparable fluctuations have been seen in smaller (6000-lipid) PM models[23] and in a number of extended simulations of simple lipid bilayers.[44] The visualization in Figure 2 suggests that the overall amplitude of the fluctuations is dependent on the simulation systems such that **PM** > **TMH** > **GPCR**. This was quantified via normalized density distribution of the lipid headgroups averaged over the course of the simulations (Figure 3). This analysis confirms that the protein-free **PM** system showed the largest fluctuations and deformations of the planar bilayer, these fluctuations becoming most pronounced over the second half of the simulation. This suggests that the large membrane deformation is not a result of the initial setup of the system, as relatively stable fluctuations are observed in the first part of the simulation before a large deformation spontaneously occurs (Figures 2 and 3a).

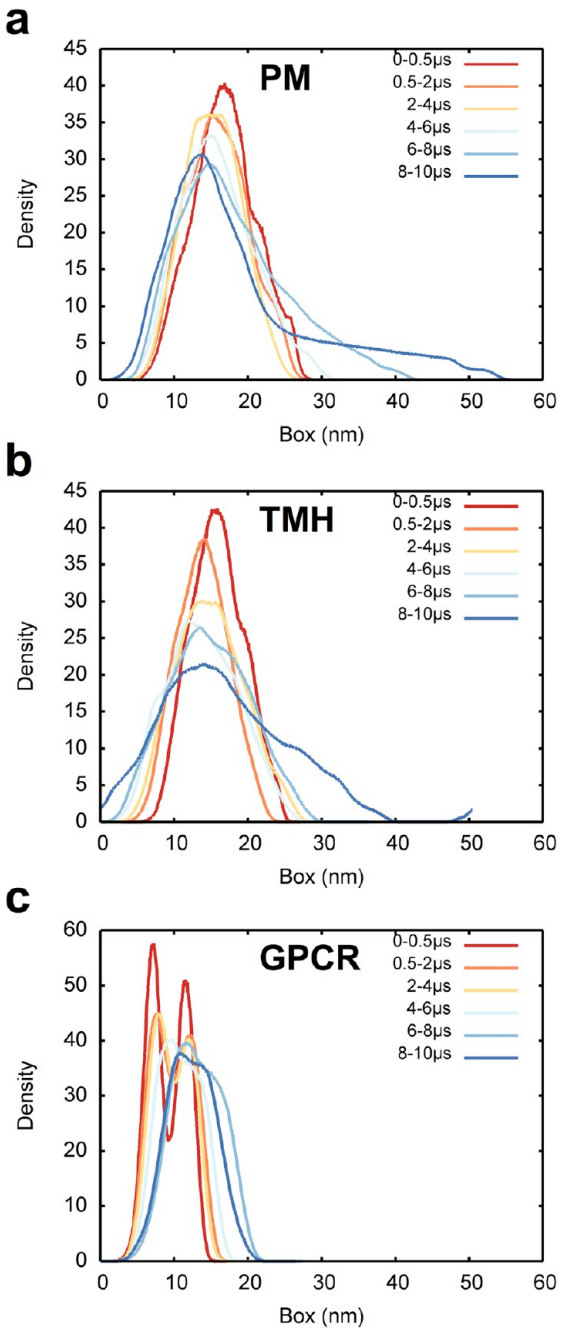

Figure 3. Lipid headgroup density distributions: density of the headgroups of all lipids except cholesterol at various intervals from (a) the **PM** simulation, (b) the **TMH** simulation, and (c) the **GPCR** simulation.

DOI: 10.1021/jacs.5b08048
J. Am. Chem. Soc. 2015, 137, 14694–14704

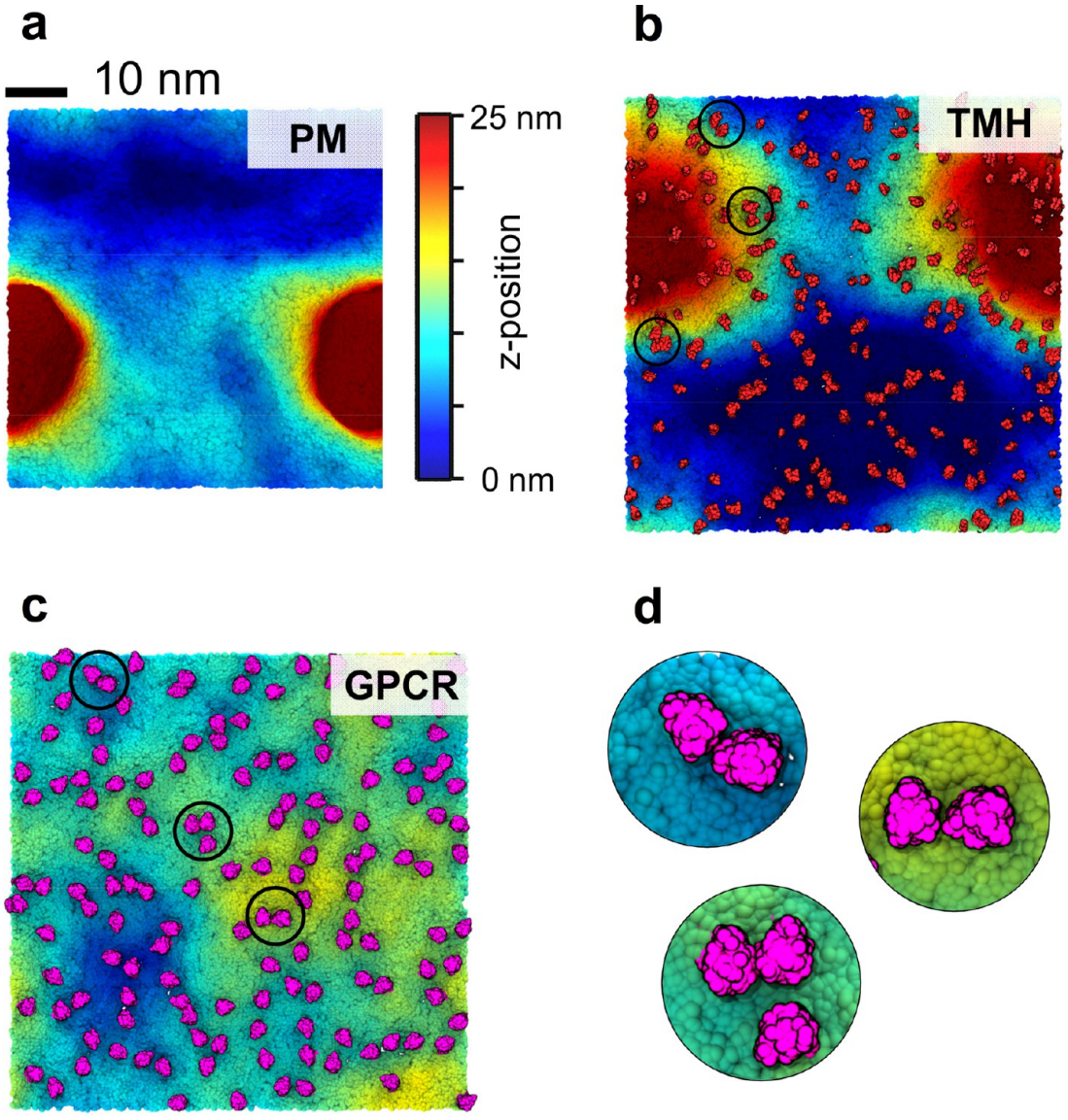

Figure 4. Membrane curvature and deformations of the three simulation systems at 10 μs. The colors correspond to the lipid headgroup's z-position using a 0 (blue) to 25 nm (red) scale. (a) **PM** system without any proteins. (b) **TMH** system with the proteins shown in red. (c) **GPCR** system with the proteins shown in pink. (d) Zoom-in on selected S1P1 oligomers within the **GPCR** system shown in (c).

Similarly, the large curvature observed for the **TMH** system (Figures 1 and 2) is reflected in the headgroup density distribution (Figure 3b).

As seen for the protein-free system, large (>40 nm)-scale fluctuations are observed throughout the **TMH** simulation, starting within the first 0.5 μs and reaching their largest extent over the final 4 μs. The curvature in the **TMH** system is less localized than in the **PM** system without any proteins, as indicated by comparison of the shapes of the 8−10 μs distributions for the two systems (Figures 1−3). Significantly, the more crowded (12% protein fractional area) **GPCR** system showed much smaller membrane fluctuations than observed for the other two simulations. This can be seen from the headgroup distribution, which reveals a bimodal structure typical of a planar bilayer projected onto the normal (i.e., z-axis) for the first half of the simulation (Figure 3c).

We further analyzed the extent of the membrane deformation by examining the final (10 μs) system configurations according to the z-positions of the lipid headgroups (Figure 4). This reveals that the **PM** system without proteins has a clear localized deformation, ∼20 nm in diameter and extending at its peak beyond 25 nm on z. A substantive (25 nm on z) deformation is also observed for the **TMH** system, but for this system (containing ca. 6% protein) the curvature is less localized and more evenly distributed throughout the system. In contrast, for the **GPCR** system, the curvature is much less localized within the plane of the bilayer and, as noted above, is of significantly smaller amplitude.

From this combination of analyses, it is clear that the presence of a complex membrane protein in a crowded system stabilizes the (mixed lipid and asymmetric) bilayer against large-amplitude fluctuations on a microsecond time scale. In principle, analysis of these fluctuations in the context of Helfrich−Canham (HC) elastic theory may be used to derive a membrane bending modulus. However, HC analysis is not strictly applicable to asymmetric membranes and so has not been applied in the current study.

DOI: 10.1021/jacs.5b08048
J. Am. Chem. Soc. 2015, 137, 14694−14704

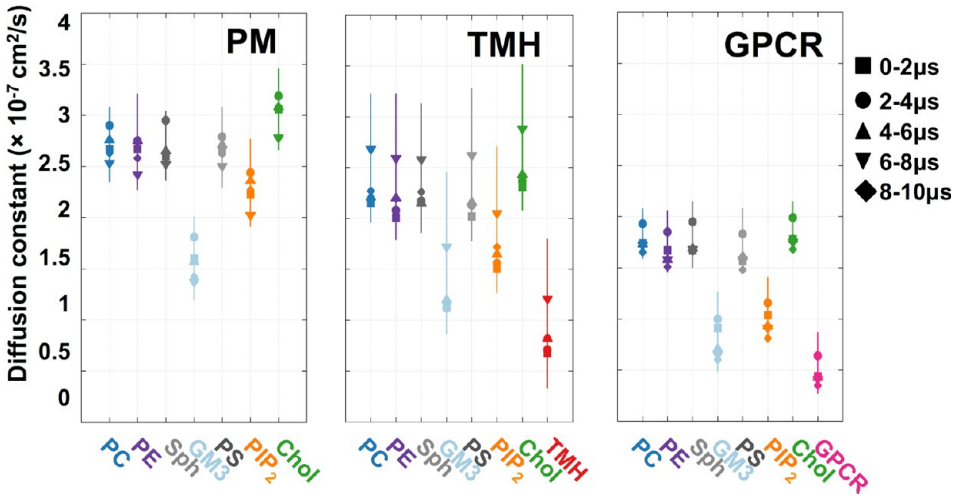

Figure 5. Lipid diffusion: lateral diffusion constant as obtained from fitting to the mean-square displacement for each lipid species and the proteins within different intervals using a time step of 5 ns for the **PM**, **THM**, and **GPCR** systems.

Since both the TM helix and the GPCR are more or less cylindrical in cross section, the "damping" effect is more likely to be a result of crowding rather than the protein shape. However, the role of the shape of TM domains (e.g., some potassium channels are conical in shape) in modulating dynamic fluctuations of membranes will be of interest to explore further.

Lipid Diffusion. To explore the local dynamics of the different lipid species and the proteins, we calculated the diffusion coefficient of the different lipids species throughout the simulations. A number of studies on simpler membrane systems, both experimental[45,46] and computational,[47−50] have indicated that crowding may slow lateral diffusion of both lipids and proteins. Diffusion coefficients were derived from mean-square displacement measurements of lipids and proteins. Within the **PM** system (i.e., without any proteins present, Figure 5) we observed slower diffusion of GM3 relative to other lipids, as previously seen in smaller membrane simulations,[23] and as has been observed for glycolipids in living cells.[16] The presence of crowded single TM helices (**TMH**, Figure 5) did not change the overall pattern of diffusion of the lipids. As anticipated the protein diffused more slowly than the lipids. However, a significant difference was observed in the presence of the GPCRs (**GPCR**, Figure 5). Overall, the crowding effect of this protein reduced lipid diffusion coefficients by a factor of ca. 1.5. This in turn suggests that the observed decrease in bilayer undulations in the presence of GPCRs is not simply a consequence of slower lipid diffusion, as the GPCR undulations after 10 μs are smaller than the PM undulations after 2 μs. This slowing of lipid diffusion was especially clear for Chol and for PIP_2. Not surprisingly given the difference in protein size, the diffusion of the S1P1 receptor is slower than was observed for the single TM domain of gp130. Overall, our calculations of lipid diffusion coefficients indicate that protein crowding slows lipid diffusion in a similar manner to that seen previously from experiments and simulations, and that this effect is more marked for those lipids (e.g., Chol, PIP_2) which interact specifically with membrane proteins. This latter observation suggests that slower lipid diffusion is because the more tightly interacting lipids diffuse together with the proteins with which they interact.

Protein−Lipid Interactions. A global picture of protein−lipid interactions may be obtained from evaluation of radial distribution function of lipids around the proteins within the two systems containing proteins (Figures 6 and S8). This analysis revealed comparable behavior between the two different protein systems, with the main protein−lipid

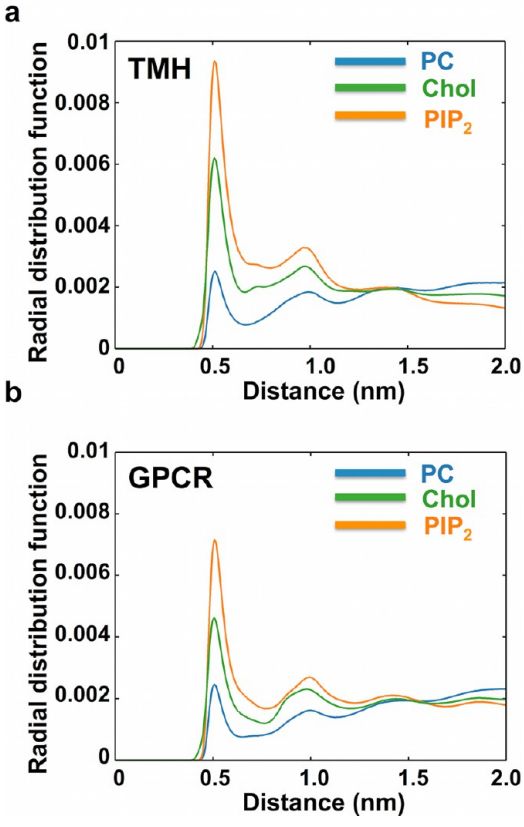

Figure 6. Protein−lipid interactions measured by the spherical radial distribution function of PC (blue), Chol (green), and PIP_2 (orange) lipid species around the protein: (a) **TMH** system and (b) **GPCR** system. The area under the curve of the radial distribution has been normalized to unity to allow for comparison between lipid species. Radial distribution functions for all lipid species are shown in Figure S8.

DOI: 10.1021/jacs.5b08048
J. Am. Chem. Soc. 2015, 137, 14694−14704

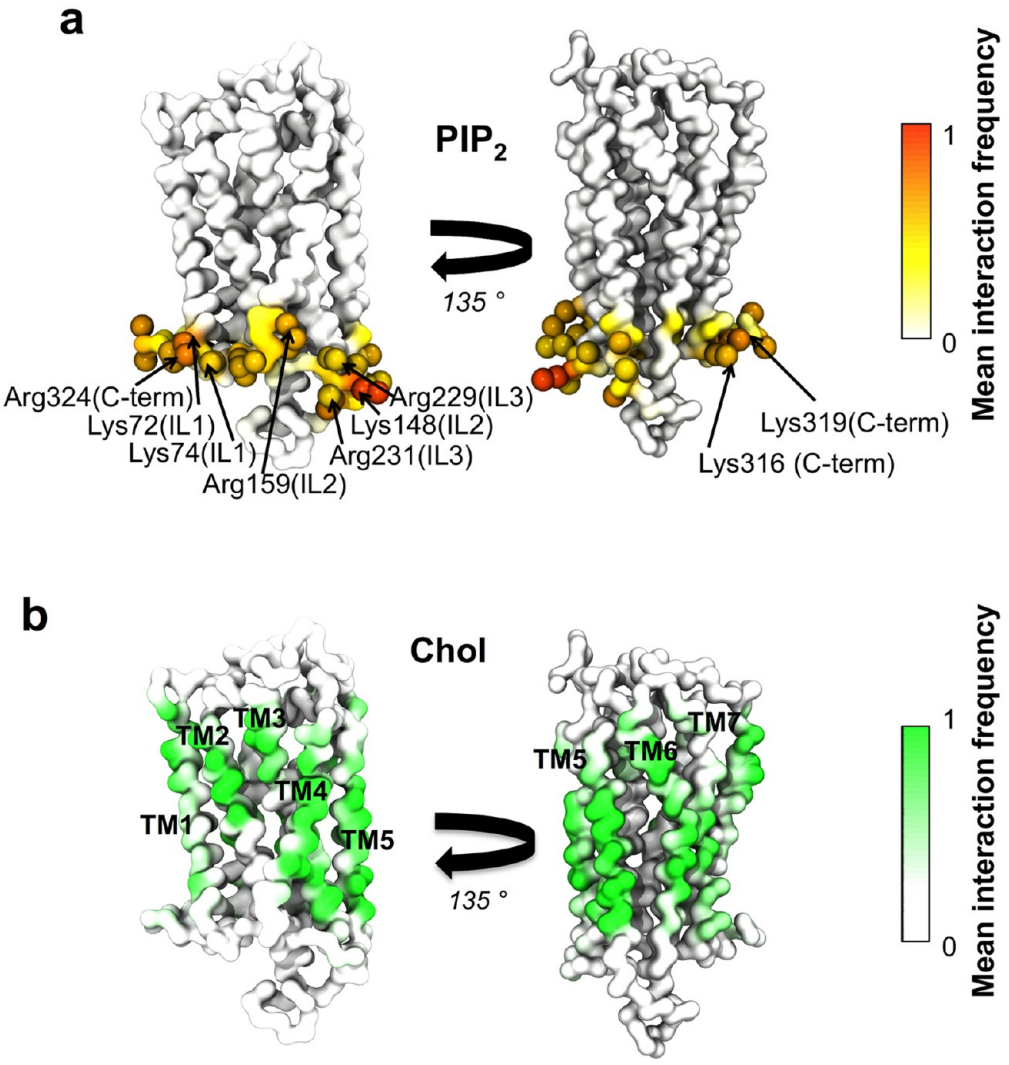

Figure 7. Protein−lipid interactions in the G-protein-coupled receptor system. Interactions between PIP_2 and Chol have been mapped onto the structure of one of the S1P1 receptors. The color scale illustrates the mean fraction of time there is an interaction with all 144 repeats of the S1P1 receptor. Thus, a value of 1 indicates a lipid forms a contact with a given residue in all proteins over the entire duration of the simulation. (a) Interactions between the phosphoryl headgroup of PIP_2 and the S1P1 receptor. Residues having interactions more than 75% of the time are shown as spheres. The basic residues within the residues are labeled. (b) Interactions between any part of the Chol molecule and the S1P1 receptor.

interactions being with PIP_2, with Chol (Figure 6), and with GM3 (Figure S8). We have explored the protein−lipid interactions pattern of the first two lipids in more detail by calculating the mean frequency of interaction between the lipid species and the different residues of each protein averaged over the entire simulation. For the **TMH** simulation we observed the pattern of behavior described previously for smaller and shorter simulations. In particular, PIP_2 was observed to form specific interactions with the C-terminal JM basic residues,[23] as has also been observed in simulations of receptor tyrosine kinase TM +JM domains in (simple) lipid bilayers[17]. For the **GPCR** system we observed clear patterns of interactions of PIP_2 and of Chol with the S1P1 receptor protein (Figure 7).

The intracellular facing surface of the S1P1 receptor is enriched in basic residues (as is frequently the case for TM proteins[6,24]). These basic residues form frequent interactions with the headgroup of PIP_2 molecules within the intracellular leaflet of the membrane, explaining the reduced mobility of PIP_2 when S1P1 receptors are present (see Figure 5). Given that the interactions between PIP_2 and the S1P1 receptors are evenly distributed around the intracellular face of the protein, the anionic lipid seems to form an annulus around the protein.[51−54] This annular interaction between PIP_2 and S1P1 receptors is found in all 144 proteins for over 75% of the simulation time, indicating that this lipid indeed forms a stable layer around the protein.

The interactions of GPCRs and Chol are of special interest, as it has been suggested that Chol is able to regulate GPCR function.[13] Cholesterol has been found to stabilize the dimerization interface of class C GPCRs,[55] and bound Chol molecules are seen in the crystal structures of a number of class A GPCRs[56,57] (although not the S1P1). We observed that hydrophobic residues on lipid-exposed surfaces of each of the TM helices of the S1P1 formed interactions with Chol over the entire simulation time in all 144 S1P1 receptors and the annulus of Chol around the GPCR (Figure 7b). Furthermore, residues on the extracellular surfaces of TM1, TM2, and TM3 formed strong interactions to the Chol headgroup (Figure S9). Interestingly, TM1, TM2, and TM3 (in addition to TM4) have been suggested to play a role in Chol-mediated dimerization of

DOI: 10.1021/jacs.5b08048
J. Am. Chem. Soc. 2015, 137, 14694−14704

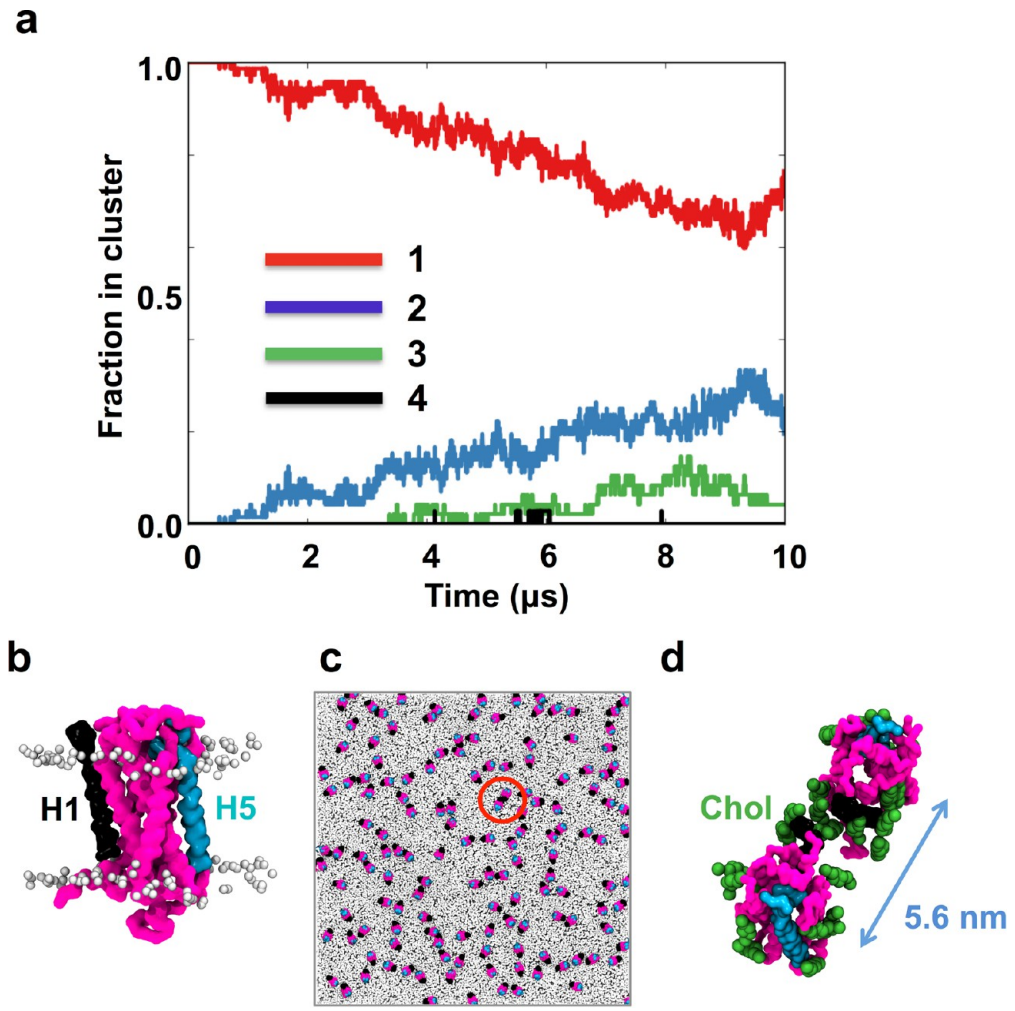

Figure 8. GPCR oligomerization. (a) Clustering of S1P1 receptors within the **GPCR** system over time. Clustering was calculated using a cutoff distance of 6.0 nm between the centers of mass of adjacent proteins. (b) S1P1 receptor (pink) with transmembrane helix 1 (H1, in black) and transmembrane helix 5 (H5, in cyan). (c) Orientation of the 144 GPCRs after 10 μs of simulation with the proteins colored as in (b), while all lipids are colored in light gray. (d) Zoom-in on one of the GPCR oligomers. Cholesterol molecules within 5 Å of the proteins are shown in green, and the distance between the centers of mass of the two proteins is shown in blue.

metabotropic glutamate receptor[55] and in the Chol binding site within β2-adrenergic receptors[56−58] based on crystal structures. Additionally, we observe a clear Chol headgroup interaction site involving two basic residues within the intracellular segments of TM5 and TM6 (Figure S9). This is of potential interest, especially as TM6 movement is believed to be involved in the main conformations change upon activation of GPCRs.[59]

The interaction between PIP_2 and protein was stable and specific, with the lipid remaining largely bound throughout the simulation for each copy of the protein (Figure S10). In contrast, Chol interacts more transient: Chol was observed to bind and dissociate throughout the simulations on a sub-microsecond time scale (Figure S11).

Protein Oligomerization. Visualization of the **TMH** simulation (Figure 4b and Movie S2) reveals oligomerization of the gp130 TM helices. In previous smaller-scale simulations, formation of TM dimers and trimers was observed.[23] Thus, the current large-scale simulations allow us to explore in more detail clustering/oligomerization of both simple (**TMH**) and more complex (**GPCR**) membrane proteins. Examination of the GPCR simulation (Figure 4c,d and Movie S3) suggests that, while for most of the time the S1P1 receptors are largely present as monomers, transient dimers can be seen, and occasionally trimeric and larger-scale clusters appear. This may be compared to, e.g., previous CG studies of rhodopsin (up to 64 proteins in a simulation) within simple model membranes, which revealed formation of linear assemblies of the GPCR.[60,61] In our simulations rather than large assembles of GPCRs we observe that the S1P1 receptor monomers come into proximity to each other, sometimes form small oligomers (dimers, trimers, etc.), which subsequently dissociate allowing monomers to diffuse away from each other (Movie S3). This association and dissociation of the S1P1 receptor monomers during the simulation suggests that a more dynamic behavior of protein−protein interactions of GPCRs may be seen when they are simulated within *in vivo*-like bilayers, compared to simpler membranes previously used computationally.

One may quantify the formation of dimers and higher oligomers during the **TMH** and **GPCR** simulations. For the **TMH** simulation within the first microsecond of the simulation more than 50% of the TM helices form dimers and higher oligomers, and after approximately 5 μs of simulation the oligomerization pattern appears to have reached a plateau (Figure S12), such that the system is a mixture of dimers,

DOI: 10.1021/jacs.5b08048
J. Am. Chem. Soc. 2015, 137, 14694−14704

trimers, and higher order oligomers in addition to a small (20% or less) fraction of monomers. Significantly, the proteins do not assemble into one large cluster, but rather exist as a mixture of smaller localized oligomers (Figure 4b). In contrast, for the GPCR simulation (Figure 8a) there is a small and slow decline in the fraction of monomeric proteins, such that in the latter part of the simulation the systems consists largely of monomers, with a small fraction of dimers (~20%) and trimers (~5%).

As discussed above, lipids form co-clusters with the proteins in both the **TMH** and the **GPCR** systems and in particular Chol, PIP_2, and GM3. A number of studies have suggested that lipid mediated effects may influence protein−protein interactions within membranes.[60,62−65] Detailed examination of S1P1 dimers observed in the **GPCR** simulation suggests that indeed Chol may mediate the protein−protein interactions (Figure 8b−d). Taken together, these results indicate that co-clustering of proteins and lipids strongly influences the dynamics and organization of the S1P1 receptor within the (model) PM.

DISCUSSION

The simulations presented here allow us for the first time to explore the dynamics of proteins and lipids at experimental length scales in an *in vivo*-like environment. The presence of large numbers of copies of membrane proteins in our simulations allows us to gather statistically significant information on protein and lipid diffusion and on protein−lipid interactions in membranes where the degree of crowding approaches that seen in cell membranes.[66] Our simulations of complex asymmetric membranes with and without membrane proteins are at length scales comparable to those accessible by experiments such as STED[16] microscopy, and the degree of complexity approaches that found in PMs.[2−4,8−10,67] These models therefore provide a valuable complement to aid interpretation of experimental data. For example, we may compare the large fluctuations in our **PM** simulations with the experimentally observed formation of blebs in regions of PM which are separated from the underlying cytoskeletal cortex.[68] Such blebs are micrometer-sized, and so the sub-micrometer scale of the large deformations observed in our simulations (performed in the absence of any model of the cytoskeletal cortex) may correlate with the early events of bleb formation.

We are able to observe differences in membrane dynamical fluctuations and in lipid diffusion depending on the system studied. In particular, the membrane proteins have a significant effect on the fluctuations and undulations of the PM. We have observed restricted movement of particular the glycolipid GM3 and of PIP_2, similar to what has been observed in smaller simulation systems.[23,25] This is in agreement with experimental observations showing anomalous diffusion of another glycolipid, GM1, in living cells.[16,69] Importantly, we see that the extent and the dynamics of protein clustering and oligomerization depend on the nature of the membrane protein embedded within the PM model. Thus, as a single TM helix from the cytokine receptor, gp130 clusters rapidly into oligomers, while a G-protein coupled receptor (GPCR), S1P1, seems to form "looser" oligomers in which the protein−protein interactions are mediated by lipids, especially Chol.

We have previously explored the effect of protein crowding on lipid mobility and complexity on smaller length scales.[23,47] Here we move closer toward simulations of biologically realistic membranes at experimentally relevant length scales. Our models still, of course, are an approximation to the membranes of living cells. In particular, we note the absence of a model of the underlying cytoskeleton from our simulations. However, since membrane compartments are believed to be in the order of 40−300 nm in size, only a small number of compartments would be present within our simulation systems, and this effect is believed to minimal.[70] Additionally, our models only contain one single protein species, which is obviously an approximation to the multiple protein species of cell membranes. The degree of crowding effect in our models is also little lower (~6−12% membrane area occupied by protein) compared to that in cell membranes, which can be up to 50% protein by mass, yielding a membrane area fraction of 25%[66] occupied by protein.

Nevertheless, these membrane models provide multiple advances compared to studies of membrane and lipid organization in smaller systems with simple membrane compositions. We are able to observe much more dynamic organization and oligomerization of GPCRs, which have previously been observed to form string-like oligomers when simulated in single lipid species (PC) bilayers.[60,61] We are able to explore specific-protein lipid interactions mediating the organization of this particular GPCR, the S1P1 receptor, within the PM model. This illustrates the importance of lipid complexity in global organization of proteins within a cell membrane. For the S1P1 receptor we can identify specific interaction sites, particularly for PIP_2 molecules within the intracellular leaflet. This may allow this signaling lipid to co-cluster with the S1P1 receptor, potentially modulating downstream signaling. Additionally, it has been shown that Chol is able to regulate the function of GPCRs,[13] and interestingly we observe a strong interaction pattern between the S1P1 receptor and Chol within our simulations. We observe specific interactions sites of the Chol headgroup around residues within TM1, TM2, and TM3. These particular helices have previously been shown to form Chol binding sites in crystal structures of both class A[56−58] and class C[55] GPCRs. In addition we also see specific interactions between Chol and intracellular basic residues within TM5 and TM6. This is an interesting observation, as TM6 is particularly believed to play a key role in the activation mechanism of GPCRs as this TM helix undergoes the largest conformation changes upon interactions with the associated G-protein.[59] Furthermore, we also observe that Chol forms an annulus around the entire membrane embedded portion of the receptor.

A possible limitation of the current study is the approximations implicit in the use of a CG force field. Although this approach captures many aspects of lipid−protein[71] and protein−protein interactions[60] within membranes, it has a number of limitations, including the use of an elastic network model, which prevents the proteins from undergoing large conformational changes, which in turn may influence their interactions. We also note that polarizable models are available for water and proteins within the MARTINI force field. However, since the lipids are currently not included in this polarizable model we have imposed a consistent level of granularity throughout the systems by using the standard (i.e., nonpolarizable) MARTINI force field.

A limitation of most current simulations—even those employing CG and related methods—is that the time scales which are achievable during simulations are so short that complex systems are unlikely to reach an equilibrium or a steady state. In the current study we can see that although the simulations are approaching a steady state, it is difficult to judge

DOI: 10.1021/jacs.5b08048
J. Am. Chem. Soc. 2015, 137, 14694−14704

whether the more complex and crowded systems are equilibrated. Future increases in computer power will help to address this limitation.

In summary, we have for the first time closed the gap between experiments and simulations in terms of both complexity and length scale at a resolution that preserves the key interactions of both the protein and lipids. The simulations presented here clearly show an agreement between dynamical behavior of lipids in living cells as illustrated by experiments[72] and the reduced mobility we observe for, e.g., GM3. Additionally, these models allow us to explore the dynamical behavior of co-clustering of proteins and lipid nanodomains. Our results illustrate that the organization of a cell membrane is controlled by various factors, and that protein−lipid interactions play a key role in organization within the plasma membrane. The models and methods presented here provide a generalizable computational approach to explore membrane proteins in more native-like lipid environments and thereby obtain an improved understanding of the local organization within the cell membranes.

■ ASSOCIATED CONTENT

Supporting Information

The Supporting Information is available free of charge on the ACS Publications website at DOI: 10.1021/jacs.5b08048.

Tables S1−S3, with details of simulation setups, and additional analysis Figures S1−S12 (PDF)

Movie S1, a 0−10 μs simulation of the **PM** system (MPG)

Movie S2, a 0−10 μs simulation of the **TMH** system (MPG)

Movie S3, a 0−10 μs simulation of the **GPCR** system (MPG)

■ AUTHOR INFORMATION

Corresponding Authors

*heidi.koldso@deshawresearch.com

*mark.sansom@bioch.ox.ac.uk

Present Address

†H.K.: D. E. Shaw Research, 120 W. 45th St., 39th Floor, New York, NY 10036

Notes

The authors declare no competing financial interest.

■ ACKNOWLEDGMENTS

Dr. Anna Duncan is acknowledged for fruitful discussions. Dr. Tom Dunton and Dr. Joseph Goose are acknowledged for the protein cluster tool. Anna Muszkiewicz is acknowledged for initial S1P1/Chol simulations. Research in M.S.P.S.'s group is funded by grants from the BBSRC, EPSRC, and the Wellcome Trust. H.K. acknowledges the Alfred Benzon foundation and the Wellcome Trust. PRACE is acknowledged for computer time.

■ REFERENCES

(1) Wenk, M. R. *Cell* **2010**, *143*, 888−895.

(2) Shevchenko, A.; Simons, K. *Nat. Rev. Mol. Cell Biol.* **2010**, *11*, 593−598.

(3) van Meer, G.; Voelker, D. R.; Feigenson, G. W. *Nat. Rev. Mol. Cell Biol.* **2008**, *9*, 112−124.

(4) van Meer, G.; de Kroon, A. I. P. M. *J. Cell Sci.* **2011**, *124*, 5−8.

(5) Zachowski, A. *Biochem. J.* **1993**, *294*, 1−14.

(6) Sharpe, H. J.; Stevens, T. J.; Munro, S. *Cell* **2010**, *142*, 158−169.

(7) Spira, F.; Mueller, N. S.; Beck, G.; von Olshausen, P.; Beig, J.; Wedlich-Soldner, R. *Nat. Cell Biol.* **2012**, *14*, 640−648.

(8) Sampaio, J. L.; Gerl, M. J.; Klose, C.; Ejsing, C. S.; Beug, H.; Simons, K.; Shevchenko, A. *Proc. Natl. Acad. Sci. U. S. A.* **2011**, *108*, 1903−1907.

(9) Coskun, Ü; Simons, K. *Structure* **2011**, *19*, 1543−1548.

(10) Lingwood, D.; Kaiser, H.; Levental, I.; Simons, K. *Biochem. Soc. Trans.* **2009**, *37*, 955−960.

(11) Rajendran, L.; Simons, K. *J. Cell Sci.* **2005**, *118*, 1099−1102.

(12) Helms, J. B.; Zurzolo, C. *Traffic* **2004**, *5*, 247−254.

(13) Zocher, M.; Zhang, C.; Rasmussen, S. G. F.; Kobilka, B. K.; Müller, D. J. *Proc. Natl. Acad. Sci. U. S. A.* **2012**, *109*, E3463−E3472.

(14) Coskun, Ü; Grzybek, M.; Drechsel, D.; Simons, K. *Proc. Natl. Acad. Sci. U. S. A.* **2011**, *108*, 9044−9048.

(15) Michailidis, I. E.; Rusinova, R.; Georgakopoulos, A.; Chen, Y.; Iyengar, R.; Robakis, N. K.; Logothetis, D. E.; Baki, L. *Pfluegers Arch.* **2011**, *461*, 387−397.

(16) Eggeling, C.; Ringemann, C.; Medda, R.; Schwarzmann, G.; Sandhoff, K.; Polyakova, S.; Belov, V. N.; Hein, B.; von Middendorff, C.; Schonle, A.; Hell, S. W. *Nature* **2009**, *457*, 1159−1162.

(17) Honigmann, A.; Mueller, V.; Ta, H.; Schoenle, A.; Sezgin, E.; Hell, S. W.; Eggeling, C. *Nat. Commun.* **2014**, *5*, 5412.

(18) Chmyrov, A.; Keller, J.; Grotjohann, T.; Ratz, M.; d'Este, E.; Jakobs, S.; Eggeling, C.; Hell, S. W. *Nat. Methods* **2013**, *10*, 737−740.

(19) Hosy, E.; Butler, C.; Sibarita, J. *Curr. Opin. Chem. Biol.* **2014**, *20*, 120−126.

(20) Sahl, S. J.; Leutenegger, M.; Hell, S. W.; Eggeling, C. *ChemPhysChem* **2014**, *15*, 771−783.

(21) Saka, S. K.; Honigmann, A.; Eggeling, C.; Hell, S. W.; Lang, T.; Rizzoli, S. O. *Nat. Commun.* **2014**, *5*, 4509.

(22) Baoukina, S.; Mendez-Villuendas, E.; Bennett, W. F. D.; Tieleman, D. P. *Faraday Discuss.* **2013**, *161*, 63−75.

(23) Koldsø, H.; Shorthouse, D.; Hélie, J.; Sansom, M. S. P. *PLoS Comput. Biol.* **2014**, *10*, e1003911.

(24) Hedger, G.; Sansom, M. S. P.; Koldsø, H. *Sci. Rep.* **2015**, *5*, 9198.

(25) Ingólfsson, H. I.; Melo, M. N.; van Eerden, F. J.; Arnarez, C.; Lopez, C. A.; Wassenaar, T. A.; Periole, X.; de Vries, A. H.; Tieleman, D. P.; Marrink, S. J. *J. Am. Chem. Soc.* **2014**, *136*, 14554−14559.

(26) van Eerden, F. J.; de Jong, D. H.; de Vries, A. H.; Wassenaar, T. A.; Marrink, S. J. *Biochim. Biophys. Acta, Biomembr.* **2015**, *1848*, 1319−1330.

(27) Koldsø, H.; Sansom, M. S. P. *J. Phys. Chem. Lett.* **2012**, *3*, 3498−3502.

(28) de Jong, D. H.; Singh, G.; Bennett, W. F. D.; Arnarez, C.; Wassenaar, T. A.; Schäfer, L. V.; Periole, X.; Tieleman, D. P.; Marrink, S. J. *J. Chem. Theory Comput.* **2013**, *9*, 687−697.

(29) Monticelli, L.; Kandasamy, S. K.; Periole, X.; Larson, R. G.; Tieleman, D. P.; Marrink, S. *J. Chem. Theory Comput.* **2008**, *4*, 819−834.

(30) Marrink, S. J.; Risselada, H. J.; Yefimov, S.; Tieleman, D. P.; de Vries, A. H. *J. Phys. Chem. B* **2007**, *111*, 7812−7824.

(31) Stansfeld, P. J.; Hopkinson, R.; Ashcroft, F. M.; Sansom, M. S. P. *Biochemistry* **2009**, *48*, 10926−10933.

(32) Hanson, M. A.; Roth, C. B.; Jo, E.; Griffith, M. T.; Scott, F. L.; Reinhart, G.; Desale, H.; Clemons, B.; Cahalan, S. M.; Schuerer, S. C.; Sanna, M. G.; Han, G. W.; Kuhn, P.; Rosen, H.; Stevens, R. C. *Science* **2012**, *335*, 851−855.

(33) Sali, A.; Blundell, T. L. *J. Mol. Biol.* **1993**, *234*, 779−815.

(34) Periole, X.; Cavalli, M.; Marrink, S.; Ceruso, M. A. *J. Chem. Theory Comput.* **2009**, *5*, 2531−2543.

(35) Scott, K. A.; Bond, P. J.; Ivetac, A.; Chetwynd, A. P.; Khalid, S.; Sansom, M. S. P. *Structure* **2008**, *16*, 621−630.

(36) Hess, B.; Kutzner, C.; van der Spoel, D.; Lindahl, E. *J. Chem. Theory Comput.* **2008**, *4*, 435−447.

(37) Berendsen, H. J. C.; Postma, J. P. M.; van Gunsteren, W. F.; DiNola, A.; Haak, J. R. *J. Chem. Phys.* **1984**, *81*, 3684−3690.

(38) Hess, B. *J. Chem. Theory Comput.* **2008**, *4*, 116−122.

(39) Levine, B. G.; Stone, J. E.; Kohlmeyer, A. *J. Comput. Phys.* **2011**, *230*, 3556−3569.
(40) Humphrey, W.; Dalke, A.; Schulten, K. *J. Mol. Graphics* **1996**, *14*, 33−38.
(41) Michaud-Agrawal, N.; Denning, E. J.; Woolf, T. B.; Beckstein, O. *J. Comput. Chem.* **2011**, *32*, 2319−2327.
(42) Rosen, H.; Stevens, R. C.; Hanson, M.; Roberts, E.; Oldstone, M. B. A. *Annu. Rev. Biochem.* **2013**, *82*, 637−662.
(43) Lukat, G.; Krüger, J.; Sommer, B. *J. Chem. Inf. Model.* **2013**, *53*, 2908−2925.
(44) Lindahl, E.; Edholm, O. *Biophys. J.* **2000**, *79*, 426−433.
(45) Ramadurai, S.; Holt, A.; Krasnikov, V.; van den Bogaart, G.; Killian, J. A.; Poolman, B. *J. Am. Chem. Soc.* **2009**, *131*, 12650−12656.
(46) Dix, J. A.; Verkman, A. S. *Annu. Rev. Biophys.* **2008**, *37*, 247−263.
(47) Goose, J. E.; Sansom, M. S. P. *PLoS Comput. Biol.* **2013**, *9*, e1003033.
(48) Javanainen, M.; Hammaren, H.; Monticelli, L.; Jeon, J.; Miettinen, M. S.; Martinez-Seara, H.; Metzler, R.; Vattulainen, I. *Faraday Discuss.* **2013**, *161*, 397−417.
(49) Domański, J.; Marrink, S. J.; Schäfer, L. V. *Biochim. Biophys. Acta, Biomembr.* **2012**, *1818*, 984−994.
(50) McGuffee, S. R.; Elcock, A. H. *PLoS Comput. Biol.* **2010**, *6*, e1000694.
(51) Lee, A. G. *Biochem. Soc. Trans.* **2011**, *39*, 761−766.
(52) Lee, A. G. *Trends Biochem. Sci.* **2011**, *36*, 493−500.
(53) Marsh, D. *Biochim. Biophys. Acta, Biomembr.* **2008**, *1778*, 1545−1575.
(54) Marsh, D.; Páli, T. *Biochim. Biophys. Acta, Biomembr.* **2004**, *1666*, 118−141.
(55) Wu, H.; Wang, C.; Gregory, K. J.; Han, G. W.; Cho, H. P.; Xia, Y.; Niswender, C. M.; Katritch, V.; Meiler, J.; Cherezov, V.; Conn, P. J.; Stevens, R. C. *Science* **2014**, *344*, 58−64.
(56) Oates, J.; Watts, A. *Curr. Opin. Struct. Biol.* **2011**, *21*, 802−807.
(57) Hanson, M. A.; Cherezov, V.; Griffith, M. T.; Roth, C. B.; Jaakola, V.; Chien, E. Y. T.; Velasquez, J.; Kuhn, P.; Stevens, R. C. *Structure* **2008**, *16*, 897−905.
(58) Stangl, M.; Schneider, D. *Biochim. Biophys. Acta, Biomembr.* **2015**, *1848*, 1886−1896.
(59) Rasmussen, S. G. F.; DeVree, B. T.; Zou, Y.; Kruse, A. C.; Chung, K. Y.; Kobilka, T. S.; Thian, F. S.; Chae, P. S.; Pardon, E.; Calinski, D.; Mathiesen, J. M.; Shah, S. T. A.; Lyons, J. A.; Caffrey, M.; Gellman, S. H.; Steyaert, J.; Skiniotis, G.; Weis, W. I.; Sunahara, R. K.; Kobilka, B. K. *Nature* **2011**, *477*, 549−555.
(60) Periole, X.; Knepp, A. M.; Sakmar, T. P.; Marrink, S. J.; Huber, T. *J. Am. Chem. Soc.* **2012**, *134*, 10959−10965.
(61) Periole, X.; Huber, T.; Marrink, S.; Sakmar, T. P. *J. Am. Chem. Soc.* **2007**, *129*, 10126−10132.
(62) Parton, D. L.; Klingelhoefer, J. W.; Sansom, M. S. *Biophys. J.* **2011**, *101*, 691−699.
(63) Dunton, T. A.; Goose, J. E.; Gavaghan, D. J.; Sansom, M. S.; Osborne, J. M. *PLoS Comput. Biol.* **2014**, *10*, e1003417.
(64) de Meyer, F. J.-M.; Rodgers, J. M.; Willems, T. F.; Smit, B. *Biophys. J.* **2010**, *99*, 3629−3638.
(65) de Meyer, F. J.; Venturoli, M.; Smit, B. *Biophys. J.* **2008**, *95*, 1851−1865.
(66) Dupuy, A. D.; Engelman, D. M. *Proc. Natl. Acad. Sci. U. S. A.* **2008**, *105*, 2848−2852.
(67) Lingwood, D.; Simons, K. *Science* **2010**, *327*, 46−50.
(68) Yanase, Y.; Carvou, N.; Frohman, M. A.; Cockcroft, S. *Biochem. J.* **2010**, *425*, 179−193.
(69) Mueller, V.; Ringemann, C.; Honigmann, A.; Schwarzmann, G.; Medda, R.; Leutenegger, M.; Polyakova, S.; Belov, V. N.; Hell, S. W.; Eggeling, C. *Biophys. J.* **2011**, *101*, 1651−1660.
(70) Kusumi, A.; Suzuki, K. G. N.; Kasai, R. S.; Ritchie, K.; Fujiwara, T. K. *Trends Biochem. Sci.* **2011**, *36*, 604−615.
(71) Stansfeld, P.; Jefferys, E.; Sansom, M. P. *Structure* **2013**, *21*, 810−819.
(72) Spillane, K. M.; Ortega-Arroyo, J.; de Wit, G.; Eggeling, C.; Ewers, H.; Wallace, M. I.; Kukura, P. *Nano Lett.* **2014**, *14*, 5390−5397.

DOI: 10.1021/jacs.5b08048
J. Am. Chem. Soc. 2015, 137, 14694−14704